(Preprint) AAS 22-687

GEOMETRIC INITIAL ORBIT DETERMINATION FROM BEARING MEASUREMENTS

Timothy Duff[*], Michela Mancini[†], Anton Leykin[‡], and John A. Christian[§]

Initial orbit determination (IOD) from only bearing measurements is a classical problem in astrodynamics. The classical solutions of Gauss, Laplace, and others can solve this problem with three bearing measurements collected at known times. In this work, we apply concepts from algebraic geometry to investigate purely geometric solutions to this same problem. It is shown that five optical sightings at unknown times may be used to determine the orbit of an unknown spacecraft. The solution only requires knowledge that the spacecraft is following a conic orbit, with no need for any orbit propagation as part of the IOD process.

INTRODUCTION

Initial orbit determination (IOD) is one of the classical problems in astrodynamics. The problem has attracted the attention of many notable mathematicians—including Gauss [1], Laplace [2], and Gibbs [3]—whose algorithms are still in widespread use hundreds of years later. The various classical IOD algorithms address different IOD scenarios. Each different IOD scenario has its own set of unique assumptions about the information available for the orbit reconstruction. Some examples are highlighted in Table 1.

What is unique about the Gibbs solution (amongst the classical algorithms) is that it is purely geometric. Specifically, it finds the 3D conic that passes through three known points in space—without any need for explicitly knowing the time at which the orbiting object resided at those three points. Similar geometric solutions have also been identified for the velocity-only IOD problem through use of the orbital hodograph [4]. To our knowledge, no such purely geometric solution exists for the angles-only scenario. Popular algorithms—including those of Gauss [1], Laplace [2], Gooding [5], and others [6]—all require the explicit use of time to propagate the body between specific points on the orbit (corresponding to the bearing measurements). Therefore, in this work we apply concepts from algebraic geometry to produce a purely geometric solution to the angles-only IOD problem. More specifically, we formulate the IOD problem in terms of solving a multivariate polynomial system of equations. Solving these equations for 5 observations (or 3 in the case of a circular orbit) reduces estimating the unknown orbital parameters to checking finitely many candidates.

Table 1. Comparison of some common IOD problem formulations.

	Gauss, Laplace, Double-R, & Gooding	**Lambert**	**Gibbs**	**Hodograph**	**This Work**
Observation type	Angles	Position	Position	Velocity	Angles
Number of observations	3	2	3	3	3 or 5
Explicit use of time	Y	Y	N	N	N

[*]NSF Postdoctoral Research Fellow, Department of Mathematics, University of Washington, Seattle, WA 98195.
[†]Graduate Research Assistant, Guggenheim School of Aerospace Engineering, Georgia Institute of Technology, Atlanta, GA 30332.
[‡]Professor, School of Mathematics, Georgia Institute of Technology, Atlanta, GA 30332.
[§]Associate Professor, Guggenheim School of Aerospace Engineering, Georgia Institute of Technology, Atlanta, GA 30332.

DISK QUADRICS AND POLYNOMIAL CONSTRAINTS FROM LINES-OF-SIGHT

In this section, we consider the representation of a space conic in terms of its disk quadric, along with a few basic related notions from projective geometry. After reviewing different parameterizations of the disk quadric, we translate line-of-sight observations into the polynomial constraints used in our approach to IOD.

Suppose we have a spacecraft in an unknown orbit that we wish to estimate. Under the assumption of classical two-body motion, the spacecraft will move along a path that is a conic section. The plane of this conic section is constrained to pass through the origin, though its orientation is unknown. Moreover, one of the conic section's foci must lie at the origin.

Now, suppose we have a set of n observations of this particle from n different observers in general position. Each observation consists of the bearing (i.e., the direction) from the observer's location to the particle's location. Thus, we have a set of n lines, with each line passing through the conic formed by the spacecraft orbit and one of the observer points. This is illustrated in Fig. 1.

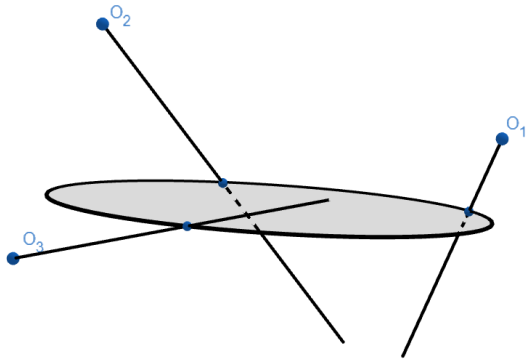

Figure 1. Illustration of geometry. The points O_i represent the observers' position and the lines the observed lines.

A 3D conic may be described in many ways. For instance, it may be represented as the intersection of a plane with a quadric surface, e.g. a cone or an ellipsoid. A less cumbersome description is the *dual representation* of the conic, which describes its locus of tangent planes. In two dimensions this is sometimes called the conic envelope, and in 3D it is usually called the *disk quadric* [7]. The reader interested in additional details on quadrics is directed to Refs. [7], [8], and [9].

Since it is both convenient and natural to work with homogeneous coordinates, we will regard a plane in space as a subset of the three-dimensional projective space $\mathbb{P}^3$. A plane in $\mathbb{P}^3$ may be represented either in *primal* terms, in which case the points on the plane are vectors in the column span of a 4×3 matrix, or in *dual* terms as the left-nullspace of 4×1 matrix $\boldsymbol{\pi}$. Similarly, a line in $\mathbb{P}^3$ may be represented in primal terms as the column span of a 4×2 matrix, or in *dual* terms, in which case the planes containing the line are vectors in the column span of a 4×2 matrix.

The disk quadric may be represented by a rank-deficient 4×4 matrix $\boldsymbol{Q}^*$. In dual terms, a plane $\boldsymbol{\pi}$ lies on the disk quadric if and only if

$$\boldsymbol{\pi}^T \boldsymbol{Q}^* \boldsymbol{\pi} = 0. \tag{1}$$

Equation (1) describes a surface in three-dimensional dual projective space. Intuitively, this surface may be viewed as an ellipsoid that has been flattened into the shape of a pancake.

An Elliptical Orbit as a Disk Quadric

We will begin by relating the disk quadric $\boldsymbol{Q}^*$ to more commonly used orbital elements. Therefore, we have an orbit whose perifocal frame is given by the orthonormal basis vectors $\{\boldsymbol{p}, \boldsymbol{q}, \boldsymbol{w}\}$. We choose the convention

where $\boldsymbol{p}$ points from the origin (located at the center of the gravitating body) to the orbit periapsis and where $\boldsymbol{w}$ is normal to the orbit plane (in the direction of the angular momentum vector). The unit vector $\boldsymbol{q}$ completes the right-handed system.

If the orbit has a semimajor axis of a and eccentricity of e, then the distance from the origin (which must lie at one of the ellipse foci) to the orbit geometric center is given by $c = ea$. Likewise, we recall that the semiminor axis b is related to a and c according to $a^2 = b^2 + c^2$. Thus, in the perifocal frame, one may write the ellipse as

$$\frac{(x+c)^2}{a^2} + \frac{y^2}{b^2} = 1, \tag{2}$$

or, equivalently,

$$b^2x^2 + 2b^2cx + b^2c^2 + a^2y^2 - a^2b^2 = 0. \tag{3}$$

Collecting terms, we may write

$$b^2x^2 + a^2y^2 + 2b^2cx + b^2(c^2 - a^2) = 0, \tag{4}$$

$$b^2x^2 + a^2y^2 + 2b^2cx - b^4 = 0. \tag{5}$$

In homogeneous coordinates $\boldsymbol{x}^T \propto [x, y, 1]$, this last equation is equivalent to

$$\boldsymbol{x}^T\boldsymbol{C}\boldsymbol{x} = 0, \tag{6}$$

where $\boldsymbol{C}$ is a nonzero 3×3 matrix given up to scale:

$$\boldsymbol{C} \propto \begin{bmatrix} b^2 & 0 & b^2c \\ 0 & a^2 & 0 \\ b^2c & 0 & -b^4 \end{bmatrix}. \tag{7}$$

If $\boldsymbol{C}$ describes the conic locus of the orbit, then $\boldsymbol{C}^* \propto \boldsymbol{C}^{-1}$ describes the conic envelope (lines tangent to the conic in the orbit plane). Therefore, recalling $a^2 = b^2 + c^2$,

$$\boldsymbol{C}^* \propto \boldsymbol{C}^{-1} = \begin{bmatrix} 1/a^2 & 0 & c/(a^2b^2) \\ 0 & 1/a^2 & 0 \\ c/(a^2b^2) & 0 & -1/(a^2b^2) \end{bmatrix} \propto \begin{bmatrix} 1 & 0 & c/b^2 \\ 0 & 1 & 0 \\ c/b^2 & 0 & -1/b^2 \end{bmatrix}. \tag{8}$$

The objective now is to relate the conic envelope to the disk quadric (a type of quadric envelope). To do this, we recall from Ref. [10] the relation

$$\boldsymbol{Q}^* \propto \boldsymbol{H}\boldsymbol{C}^*\boldsymbol{H}^T \tag{9}$$

where, in this case, one may compute $\boldsymbol{H}$ as the 4×3 matrix

$$\boldsymbol{H} = \begin{bmatrix} \boldsymbol{p} & \boldsymbol{q} & \boldsymbol{0}_{3\times1} \\ 0 & 0 & 1 \end{bmatrix}. \tag{10}$$

Performing the requisite multiplications gives a disk quadric of

$$\boldsymbol{Q}^* \propto \boldsymbol{H}\boldsymbol{C}^*\boldsymbol{H}^T \tag{11}$$

$$= \begin{bmatrix} \boldsymbol{p} & \boldsymbol{q} & (c/b^2)\boldsymbol{p} \\ (1/b^2) & 0 & (-1/b^2) \end{bmatrix} \begin{bmatrix} \boldsymbol{p}^T & 0 \\ \boldsymbol{q}^T & 0 \\ \boldsymbol{0}_{1\times3} & 1 \end{bmatrix} \tag{12}$$

$$= \begin{bmatrix} \boldsymbol{p}\boldsymbol{p}^T + \boldsymbol{q}\boldsymbol{q}^T & (c/b^2)\boldsymbol{p} \\ (c/b^2)\boldsymbol{p}^T & (-1/b^2) \end{bmatrix}. \tag{13}$$

Thus,

$$\boldsymbol{Q}^* \propto \begin{bmatrix} \boldsymbol{p}\boldsymbol{p}^T + \boldsymbol{q}\boldsymbol{q}^T & (c/b^2)\boldsymbol{p} \\ (c/b^2)\boldsymbol{p}^T & (-1/b^2) \end{bmatrix} = \begin{bmatrix} \boldsymbol{I}_{3\times3} - \boldsymbol{w}\boldsymbol{w}^T & (c/b^2)\boldsymbol{p} \\ (c/b^2)\boldsymbol{p}^T & (-1/b^2) \end{bmatrix}. \tag{14}$$

Consequently, the 4×4 matrix $\boldsymbol{Q}^*$ describing the disk quadric consists of two scalars (b and c, which describe the size and shape of the orbit in the perifocal plane) and the two orthonormal vectors that span the perifocal plane ($\boldsymbol{p}$ and $\boldsymbol{q}$). Since $\boldsymbol{p}$ and $\boldsymbol{q}$ are orthonormal, we have the three constraints

$$\boldsymbol{p}^T\boldsymbol{p} = \boldsymbol{q}^T\boldsymbol{q} = 1, \quad \boldsymbol{p}^T\boldsymbol{q} = 0. \tag{15}$$

The two parameterizations of $\boldsymbol{Q}^*$ from Eq. (14) and the three constraints from Eq. (15) were also given in Ref. [11]. The difficulty with these specific ways of writing $\boldsymbol{Q}^*$ is that they require different treatment for an elliptical orbit (when the direction of $\boldsymbol{p}$ is well-defined) and for a circular orbit (when the direction of $\boldsymbol{p}$ is *not* well-defined). Thus, we introduce a third parameterization of $\boldsymbol{Q}^*$ that avoids this deficiency. Specifically, define the vector $\boldsymbol{g} = (c/b^2)\boldsymbol{p}$, which is well-defined for both elliptical and circular orbits. We observe, in the limit as $e \to 0$, that $c \to 0$ and $\boldsymbol{g} \to \boldsymbol{0}_{3\times 1}$. Therefore, we may parameterize the disk quadric as

$$\boldsymbol{Q}^* \propto \begin{bmatrix} \boldsymbol{I}_{3\times 3} - \boldsymbol{w}\boldsymbol{w}^T & \boldsymbol{g} \\ \boldsymbol{g}^T & (-1/b^2) \end{bmatrix}, \tag{16}$$

where the parameters $\boldsymbol{w}, \boldsymbol{g}, b$ satisfy the two constraints

$$\boldsymbol{w}^T\boldsymbol{w} = 1, \quad \boldsymbol{w}^T\boldsymbol{g} = 0. \tag{17}$$

Thus, because of its benefits for near-circular orbits, the parameterization of $\boldsymbol{Q}^*$ from Eq. (16) is used in the developments that follow.

Observation Lines and Tangent Planes

Recall that a plane in $\mathbb{P}^3$, represented by $\boldsymbol{\pi} \in \mathbb{R}^{4\times 1}$, is tangent to $\boldsymbol{Q}$ if and only if

$$\boldsymbol{\pi}^T\boldsymbol{Q}^*\boldsymbol{\pi} = 0. \tag{18}$$

Observed lines $\boldsymbol{\ell}_1, \ldots, \boldsymbol{\ell}_n \subset \mathbb{P}^3$ must lie within the unknown tangent planes $\boldsymbol{\pi}_1, \ldots, \boldsymbol{\pi}_n$, obtained geometrically as the join of each observed line with the corresponding tangent line in the orbit plane. Each $\boldsymbol{\pi}_i$ constructed in this way is the unique plane in $\boldsymbol{Q}^*$ that contains $\boldsymbol{\ell}_i$. This can be appreciated in Fig. 2.

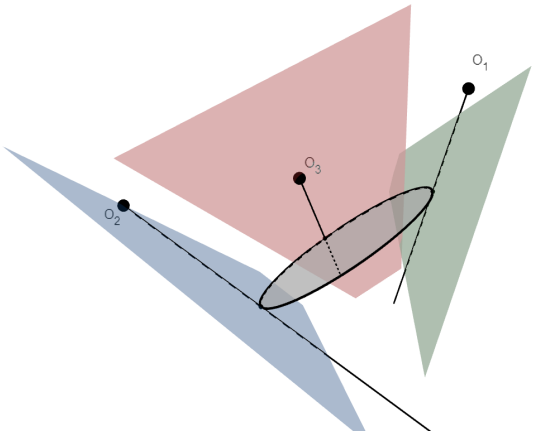

Figure 2. Representation of the planes $\boldsymbol{\pi}_1, \boldsymbol{\pi}_2, \boldsymbol{\pi}_3$ of the disk quadric containing three observed lines from the three observers O_1, O_2 and O_3.

Each observed line $\boldsymbol{\ell}_i$ may be described in primal coordinates as the column space of the 4×2 matrix

$$\begin{bmatrix} \boldsymbol{x}_i & \boldsymbol{u}_i \\ 1 & 0 \end{bmatrix}. \tag{19}$$

Here $\boldsymbol{x}_i \in \mathbb{R}^3$ gives the coordinates of the observer point O_i and $\boldsymbol{u}_i \in \mathbb{R}^3$ is a *bearing* measurement. The bearings, in noiseless scenarios, are unit vectors pointing from observers towards points on the orbit.

A dual representation of the line $\boldsymbol{\ell}_i$ is given by *any* full-rank 4×2 matrix $\boldsymbol{A}_i$ such that

$$\boldsymbol{A}_i^T \begin{bmatrix} \boldsymbol{x}_i & \boldsymbol{u}_i \\ 1 & 0 \end{bmatrix} = \mathbf{0}_{2\times 2}. \tag{20}$$

Many choices are possible for the matrix $\boldsymbol{A}_i$ giving the dual representation of $\boldsymbol{\ell}_i$. In the next subsection, we explain two methods—one algebraic, the other numerical—by which a suitable $\boldsymbol{A}_i$ may be directly computed from observations. Once we are given the matrix $\boldsymbol{A}_i$, the tangent plane $\boldsymbol{\pi}_i$ may be written as

$$\boldsymbol{\pi}_i = \boldsymbol{A}_i \boldsymbol{c}_i \tag{21}$$

for some nonzero 2×1 vector $\boldsymbol{c}_i$. Substituting this expression into equation (18) yields

$$\boldsymbol{c}_i^T \boldsymbol{A}_i^T \boldsymbol{Q}^* \boldsymbol{A}_i \boldsymbol{c}_i = 0. \tag{22}$$

The vector $\boldsymbol{c}_i$, which depends on the unknown tangent plane, may be eliminated from this equation to obtain a constraint depending only on the observed line and the unknown entries of the disk quadric: namely,

$$\det\left(\boldsymbol{A}_i^T \boldsymbol{Q}^* \boldsymbol{A}_i\right) = 0. \tag{23}$$

Thus, each of the observed lines $\boldsymbol{\ell}_1, \ldots, \boldsymbol{\ell}_n$ places a constraint on the 3D conic that is polynomial in the entries of $\boldsymbol{A}_i$ and $\boldsymbol{Q}^*$. These are the basic constraints from which we may determine the unknown orbit.

Dual representation of an observed line

The dual representation of the line $\boldsymbol{\ell}_i$ is given by the matrix $\boldsymbol{A}_i$. To express $\boldsymbol{A}_i$ algebraically in terms of the observer vector $\boldsymbol{x}_i$ and the bearing vector $\boldsymbol{u}_i$, it is convenient to partition the primal matrix into two square blocks, $\boldsymbol{S}_1, \boldsymbol{S}_2 \in \mathbb{R}^{2\times 2}$:

$$\begin{bmatrix} \boldsymbol{x}_i & \boldsymbol{u}_i \\ 1 & 0 \end{bmatrix} = \begin{bmatrix} \boldsymbol{S}_1 \\ \boldsymbol{S}_2 \end{bmatrix}. \tag{24}$$

Assuming the observations $\boldsymbol{x}_i, \boldsymbol{u}_i$ are sufficiently generic, then both $\boldsymbol{S}_1$ and $\boldsymbol{S}_2$ will be invertible. Thus, application of Eq. (20) allows us to parameterize $\boldsymbol{A}_i$ as

$$\boldsymbol{A}_i^T = \left[\boldsymbol{A}_1' \;\middle|\; -\boldsymbol{A}_1' \boldsymbol{S}_1 \boldsymbol{S}_2^{-1}\right], \tag{25}$$

where $\boldsymbol{A}_i'$ may be chosen to be any invertible 2×2 matrix. Write $\boldsymbol{x}_i = \begin{bmatrix} x_{i,1} & x_{i,2} & x_{i,3} \end{bmatrix}^T$ and $\boldsymbol{u}_i = \begin{bmatrix} u_{i,1} & u_{i,2} & u_{i,3} \end{bmatrix}^T$. Noting that $\det \boldsymbol{S}_2 = u_3$,, we find it convenient to make the choice $\boldsymbol{A}_1' = u_3 \boldsymbol{I}_{2\times 2}$. Using these conventions we compute

$$\boldsymbol{A}_i' \boldsymbol{S}_1 \boldsymbol{S}_2^{-1} = \begin{bmatrix} x_{i,1} & u_{i,1} \\ x_{i,2} & u_{i,2} \end{bmatrix} \begin{bmatrix} 0 & -u_{i,3} \\ -1 & x_{i,3} \end{bmatrix} = \begin{bmatrix} -u_{i,1} & x_{i,3}u_{i,1} - x_{i,1}u_{i,3} \\ -u_{i,2} & x_{i,3}u_{i,2} - x_{i,2}u_{i,3} \end{bmatrix}, \tag{26}$$

and hence

$$\boldsymbol{A}_i = \begin{bmatrix} u_{i,3} & 0 \\ 0 & u_{i,3} \\ u_{i,1} & u_{i,2} \\ x_{i,1}u_{i,3} - x_{i,3}u_{i,1} & x_{i,2}u_{i,3} - x_{i,3}u_{i,2} \end{bmatrix}. \tag{27}$$

A numerical alternative to the dual representation given by (27) may be obtained from the singular value decomposition (SVD) of the transposed primal matrix,

$$\begin{bmatrix} \boldsymbol{x}_i^T & 1 \\ \boldsymbol{u}_i^T & 0 \end{bmatrix} = \boldsymbol{U}_i \boldsymbol{\Sigma} \boldsymbol{V}_i^T = \boldsymbol{U}_i \begin{bmatrix} \sigma_{i,1} & 0 \\ 0 & \sigma_{i,2} \\ 0 & 0 \\ 0 & 0 \end{bmatrix} \begin{bmatrix} \boldsymbol{v}_{i,1} & \boldsymbol{v}_{i,2} & \boldsymbol{v}_{i,3} & \boldsymbol{v}_{i,4} \end{bmatrix}^T.$$

Thus, since $\boldsymbol{A}_i$ must lie in the null space of the transposed primal matrix, we may select $\boldsymbol{A}_i$ using the last two columns of $\boldsymbol{V}_i$,

$$\boldsymbol{A}_i = \begin{bmatrix} \boldsymbol{v}_{i,3} & \boldsymbol{v}_{i,4} \end{bmatrix}^T. \tag{28}$$

ORBIT DETERMINATION VIA POLYNOMIAL SYSTEM SOLVING

Formulation as a polynomial system of equations

If we take a scaling factor of 1 in the parameterization of $\boldsymbol{Q}^*$ given in equation (16), the 7 unknown orbital parameters $\boldsymbol{w}, \boldsymbol{g}, b$ will be solutions to a system of $2 + n$ equations given by (17) and (23) for $i = 1, \ldots, n$. For *sufficiently generic* observations, we expect that when $7 = 2 + n$, or $n = 5$, this system of equations will have finitely many solutions. In fact, we expect the number of solutions to be *constant* if we count over the complex numbers. Such a "number conservation" principle may be viewed as a generalization of the fundamental theorem of algebra, which treats the case of a single polynomial in a single unknown. A formal statement in the language of algebraic geometry may be found, for instance, in Ref. [12, Theorem 2.29].

In the preceding paragraph, the precise meaning of the phrase "sufficiently generic" is that the vector of all observations $\begin{bmatrix} \boldsymbol{x}_1^T | \cdots | \boldsymbol{x}_5^T \mid \boldsymbol{u}_1^T | \cdots | \boldsymbol{u}_5^T \end{bmatrix} \in \mathbb{R}^{30}$ lies outside of an appropriately-defined *discriminant locus*. This discriminant locus is analogous to the commonly-known discriminant of a quadratic equation, but very difficult to describe explicitly (e.g., see [13, Sec. 3.1] for an example with two unknowns.)

To see an example which is *not* sufficiently generic, we may consider any 5 observations from any perfectly-circular orbit. In this case, the true orbit satisfies $\boldsymbol{g} = 0$ and the corresponding solution is *singular*; that is, the 7×7 Jacobian matrix of the system evaluated at this solution is rank-deficient. Such a singular solution may be difficult to estimate accurately with standard numerical methods. The same is true for the nearly-singular solutions arising from the practical case of nearly-circular orbits.

On the other hand, if we enforce the constraint of a circular orbit by requiring that $\boldsymbol{w} = 0$, then $n = 3$ observations suffice to recover the orbit up to finitely many possibilities. Under this circular model, we obtain another system of polynomial equations, from which we may compute the remaining orbital parameters $\boldsymbol{w}, b$. Such a model has the advantage of needing fewer observations, and may potentially give a reasonable approximation of the true orbit in the nearly-circular case.

We summarize the two different orbit models, the associated polynomial systems, and how many solutions they have for generic data in Proposition 1.

Proposition 1.

1. For $n = 5$ generic observations $(\boldsymbol{x}_i, \boldsymbol{u}_i)_{i=1}^5$, the *elliptical model* given by equations (17) and (23) for $i = 1, \ldots, 5$ has a total of $\mathbf{66}$ complex solutions in the unknown matrix $\boldsymbol{Q}^*$, each lifting to 4 solutions $(\pm\boldsymbol{w}, \boldsymbol{g}, \pm b)$ in terms of the parameterization (16).
2. For $n = 3$ generic observations $(\boldsymbol{x}_i, \boldsymbol{u}_i)_{i=1}^3$, the *circular model* given by equations (23) for $i = 1, \ldots, 3$, plus the additional constraints
$$\boldsymbol{w}^T\boldsymbol{w} = 1, \quad \boldsymbol{g} = 0, \tag{29}$$
has a total of $\mathbf{12}$ complex solutions in the unknown matrix $\boldsymbol{Q}^*$, each lifting to 4 solutions $(\pm\boldsymbol{w}, 0, \pm b)$ in terms of the parameterization (16).

The claims appearing in Proposition 1 regarding the number of solutions may be readily verified using any one of the standard methods for solving polynomial systems, such as Gröbner bases (see [14, Ch. 2] for an overview), or polynomial homotopy continuation [15]. In our experiments, we solve the systems associated to either model using an implementation of the latter method provided by the software package `NAG4M2` [16] in the computer algebra system `Macaulay2` [17]. We give an overview of homotopy continuation in the next subsection.

Remark 1. For different choices of real parameters $(\boldsymbol{x}_i, \boldsymbol{u}_i)_{i=1}^n$, the systems appearing in Proposition 1 may have one or more *real* solutions. For either of our two models, the precise notion of "real solution" turns out

to depend on which quantities are considered as unknowns. For example, the real disk quadric given by

$$\boldsymbol{Q}^* = \begin{bmatrix} 3/2 & 12 & 0 & 1 \\ 1/2 & 3/2 & 0 & 0 \\ 0 & 0 & 1 & 0 \\ 1 & 0 & 0 & -1 \end{bmatrix}$$

can only be lifted to the complex-valued parameters

$$\boldsymbol{w}^T = (\pm i/\sqrt{2}) \begin{bmatrix} 1 & 1 & 0 \end{bmatrix}, \quad \boldsymbol{g}^T = \begin{bmatrix} 1 & 0 & 0 \end{bmatrix}, \quad b = \pm 1.$$

Solving polynomial systems with parameter homotopies

Numerical homotopy continuation is a general method which can be used to solve polynomial systems, such as those appearing in Proposition 1. The essential idea underlying the method is as follows: since the roots of polynomials vary continuously with their coefficients, we can use a system whose solution set is known (the *start system*) to solve some other system in the same class of systems (the *target system*) by estimating how the solutions change (*path-tracking*) as we deform one system into another. We use a short example to illustrate the main ideas.

Example 1. To solve the target system in two variables $\boldsymbol{X} = \begin{bmatrix} x & y \end{bmatrix}^T$ given by

$$\boldsymbol{F}_1(\boldsymbol{X}) = \begin{bmatrix} -x^3 + 2\,x + 1 & -y^2 + x + 1 \end{bmatrix}^T = 0,$$

we may use the well-known *total-degree* start system [15, Sec. 8.4.1]

$$\boldsymbol{F}_0(\boldsymbol{X}) = \begin{bmatrix} x^3 - 1 & y^2 - 1 \end{bmatrix}^T = 0,$$

and the straight-line homotopy

$$\boldsymbol{H}(\boldsymbol{X}; t) = (1 - t)\,\boldsymbol{F}_0(\boldsymbol{X}) + t\,\boldsymbol{F}_1(\boldsymbol{X}) = 0,$$

The 6 start solutions have the form $\begin{bmatrix} e^{2\pi i k/3} & \pm 1 \end{bmatrix}^T$ for $k = 1, 2, 3$. Each determines an initial value for a *solution path* $\boldsymbol{X}(t)$, defined for t near 0, which satisfies $H(\boldsymbol{X}(t); t) = 0$. For this particular homotopy, each solution path is defined for all $t \in [0, 1]$, and each value $\boldsymbol{X}(1)$ gives one of the six target solutions. For instance, if $\boldsymbol{X}(0) = \begin{bmatrix} 1 & 1 \end{bmatrix}^T$, then $\boldsymbol{X}(1) \approx \begin{bmatrix} .246, -.712 \end{bmatrix}^T$.

The choice of the start system is an important factor when implementing any homotopy continuation method. Usually, we want a start system that is general enough to solve any possible target system coming from a specific application. Another important factor when choosing a start system is its *specificity*, or the number of start solutions. Different choices of start systems are compared in Ref. [15, Ch. 8], where a basic tradeoff is identified: a start system that is easy to describe and solves a large class of systems will typically require tracking more paths. For example, if the total-degree start system is used to solve an instance of the elliptical model, this requires tracking $4^5 \cdot 2^2 = 4096$ paths. This should be compared with the optimal number of 66 established by Proposition 1. If the total degree homotopy was to be used to solve the elliptical model, then we would need to track $4096 - 66 = 4030$ *divergent* solution paths with $|\boldsymbol{X}(t)| \to \infty$ as $t \to 1^-$.

In contrast to the total degree homotopy, *parameter homotopies* [18] allow us to track, under reasonable assumptions, the optimal number of paths. Since "most" instances of the systems in Proposition 1 will have the same number of solutions, any randomly-chosen instance may, in principle, be chosen as a start system. Parameter homotopies may be used in a general setting where we have a system $\boldsymbol{F}(\boldsymbol{X}; \boldsymbol{P}) = 0$, with as many equations as unknowns, which depends polynomially both on the unknowns $\boldsymbol{X}$ and certain *parameters* $\boldsymbol{P}$ depending on the observations. For the systems of interest to us, there is some flexibility in how these parameters are chosen. One simple choice is that the target parameters $\boldsymbol{P}_1 \in \mathbb{R}^{8n}$ consist of all dual coordinates of all n lines—that is, $\boldsymbol{P}_1 \in \mathbb{R}^{40}$ for the elliptical model, and $\boldsymbol{P}_0 \in \mathbb{R}^{24}$ for the circular model.

Alternatively, using equation 27, we may directly encode the observer and bearing vectors into a parameter vector $\boldsymbol{P}_1 \in \mathbb{R}^{6n}$—that is, $\boldsymbol{P}_1 \in \mathbb{R}^{30}$ for the elliptical model, and $\boldsymbol{P}_1 \in \mathbb{R}^{18}$ for the circular model. The following description of parameter homotopies applies equally well to either choice.

In general, the parameter values $\boldsymbol{P}_1$ encoded by a set of observations specify the target system $\boldsymbol{F}(\boldsymbol{X}; \boldsymbol{P}_1) = 0$ of the parameter homotopy. If there are m parameter values, ie $\boldsymbol{P}_1 \in \mathbb{R}^m$, then the start system should also be a $m \times 1$ vector $\boldsymbol{P}_0$. For the start system $\boldsymbol{F}(\boldsymbol{X}; \boldsymbol{P}_0) = 0$, we are given a pre-computed set of $d \in \{12, 66\}$ complex solutions $\boldsymbol{X}_1(0), \ldots, \boldsymbol{X}_d(0)$ whose coordinates are the unknown orbital elements which are pairwise-inequivalent up to the sign-symmetries described in Proposition 1. To extend these start solutions to *solution paths* $\boldsymbol{X}_1(t), \ldots, \boldsymbol{X}_d(t)$, we "deform" the start system into the target system via the parameter homotopy

$$\boldsymbol{H}(\boldsymbol{X}; \boldsymbol{P}, t) = \boldsymbol{F}(\boldsymbol{X}; t\boldsymbol{P}_1 + (1-t)\boldsymbol{P}_0) = 0. \tag{30}$$

Each solution path $\boldsymbol{X}(t)$ is an implicit function of t satisfying (30) and the nonlinear ODE system

$$\frac{d\boldsymbol{H}}{d\boldsymbol{X}} \frac{d\boldsymbol{X}}{dt} + \frac{d\boldsymbol{H}}{dt} = 0. \tag{31}$$

This ODE, together with one of the start solutions $\boldsymbol{X}_i(0)$, gives an initial value problem for an unknown solution path $\boldsymbol{X}_i(t)$ satisfying (30). Numerical integration methods allow us to estimate $\boldsymbol{X}_i(t)$ for $t \in [0, 1]$. In practice, we approximate a solution path using numerical/predictor corrector methods. If $\boldsymbol{X}_i(t)$ is known within some tolerance for some $t \in [0, 1]$, then a "predictor step" (typically the standard fourth-order Runge-Kutta method) uses (31) to find an initial estimate for $\boldsymbol{X}_i(t + \Delta t)$ for some step-size Δt. This estimate is subsequently refined by a "corrector step" using one or more iterations of Newton's method.

A key property of parameter homotopies is that, under mild hypotheses, they are *globally convergent with probability-one.* The following key properties of the parameter homotopy (30) are consequences of a more general parameter continuation theorem [15, Theorem 7.1.1]. We specialize this general result to our case of particular interest. For sufficiently generic (and hence, *almost all*) $(\boldsymbol{P}_0, \boldsymbol{P}_1)$, we have:

1. Each start solution $\boldsymbol{X}_i(0)$ extends to a solution path $\boldsymbol{X}_i(t)$ which is smooth for all $t \in [0, 1]$.
2. Every solution to the target system may be obtained up to sign-symmetry from the *endpoint* $\boldsymbol{X}_i(1)$ of some solution path $\boldsymbol{X}_i(t)$.

At this point, it is worth pointing out key differences between homotopy continuation, a *global* root-finding method, from a more standard *local* approach like Newton's method. In Newton's method, we would pick a single "start solution" $\boldsymbol{X}$, then compute iterates $\boldsymbol{X} \leftarrow \boldsymbol{X} - \boldsymbol{F}(\boldsymbol{X}; \boldsymbol{P}_1)$ until some convergence condition is satisfied, yielding a single solution to the target system $\boldsymbol{F}(\boldsymbol{X}; \boldsymbol{P}_1) = 0$. In practice, this may suffer if $\boldsymbol{X}$ is not sufficiently close to a target solution.

In homotopy continuation, "start solutions" instead refer to solutions to the start system $\boldsymbol{F}(\boldsymbol{X}; \boldsymbol{P}_0) = 0$ which have been pre-computed. There is no requirement that these start solutions be "close" to solutions of the target system, nor that the start and target parameters be close in the space of all parameters. As long as the pre-computed start parameters $\boldsymbol{P}_0 \in \mathbb{C}^m$ are *sufficiently generic*, all start solutions can be numerically continued from $t = 0$ to $t = 1$. Thus, we can compute *all* solutions to the target system $\boldsymbol{F}(\boldsymbol{X}; \boldsymbol{P}_1) = 0$, provided that the target parameters $\boldsymbol{P}_1$ are also sufficiently generic.

Usually, choosing random complex numbers for the start parameters $\boldsymbol{P}_0$ will be sufficient to ensure that all isolated solutions of the target system specified by $\boldsymbol{P}_1$ can be computed. As such, the choice of start parameters, provided that they are sufficiently random, may be expected to have relatively little impact on the accuracy of the computed target solutions. Here, "accuracy" may be defined in one of two ways: either, in the noiseless setting, the distance between a "ground truth" target solution and the approximation that is computed by homotopy continuation, or by the distance from the noiseless ground truth to a solution after noise is introduced. Generally, we expect the former quantity to be small, while the latter quantity depends on the amount of noise and the problem formulation. In either case, there is no clear, simple criterion for

picking a "good" start system that may lead to more accurate results. However, there are some properties of the start parameters that we can aim to optimize. For instance, if the Jacobian matrices $\frac{d\boldsymbol{H}}{d\boldsymbol{X}}(\boldsymbol{X}_i(0); \boldsymbol{P}_0)$ are well-conditioned for each of the start solutions $\boldsymbol{X}_i(0)$, then for each solution path we can expect the predictor/corrector steps to be more accurate when t is near 0. With this in mind, our choice of start system was based on generating several different sets of parameters $\boldsymbol{P}_0$ at random, with coordinates drawn uniformly from the complex unit circle, computing a complete set of solutions for each system, and selecting the system whose maximum condition number over all solutions was smallest. To solve the parametric systems in each model for an initial set of parameters, we used an approach based on monodromy, which works well in tandem with parameter homotopies and can naturally exploit the four-fold symmetry in solutions. We refer to [19, 20, 21] for more details about this approach.

In our implementation, we use the numerical formula 28 to determine the parameters representing the dual coordinates of each line-of-sight observation. Before solving, we rescale all distance measurements into units of earth-radii, which has the typical effect of making the entries of $\boldsymbol{Q}^*$ comparable in magnitude. We use the default path-tracker settings in `NAG4M2`, except that a minimum stepsize of $\Delta t = 1 \times 10^{-16}$ is used. Additionally, we handle (infrequent) cases of path failure for $t \approx 1$ using Cauchy's endgame for estimating singular solutions [15, Ch. 10].

EXPERIMENTS

Throughout our experiments, we consider an orbit with known parameters, the *ground-truth* solution, represented as the disk quadric $\boldsymbol{Q}^*$. All distances are computed in units of earth-radii so that the entries of $\boldsymbol{Q}^*$ are comparable in magnitude. To estimate the ground-truth from the d solutions computed by the homotopy continuation solver, represented by disk quadrics $\widehat{\boldsymbol{Q}_1^*}, \ldots, \widehat{\boldsymbol{Q}_d^*}$, we take the closest solution

$$\widehat{\boldsymbol{Q}^*} = \underset{\widehat{\boldsymbol{Q}_1^*},\ldots,\widehat{\boldsymbol{Q}_d^*}}{\arg\min} ||\widehat{\boldsymbol{Q}_i^*} - \boldsymbol{Q}^*||_2, \tag{32}$$

where $||\bullet||_2$ denotes the ℓ_2 Hermitian vector norm on the complex vector space of 4×4 symmetric matrices,

$$||\boldsymbol{Q}^*|| = \sqrt{\sum_{1 \leqslant i \leqslant j \leqslant 4} |\boldsymbol{Q}^*_{i,j}|^2}.$$

We measure the error in the estimate of $\boldsymbol{Q}^*$ given in (32) with an absolute error:

$$\Delta Q^* = ||\widehat{\boldsymbol{Q}^*} - \boldsymbol{Q}^*||_2, \tag{33}$$

Additionally, we will compare the ground-truth classical orbital elements $(a, e, i, \Omega, \omega)$ to their estimates $(\widehat{a}, \widehat{e}, \widehat{i}, \widehat{\Omega}, \widehat{\omega})$. Here Ω denotes the longitude of the mean. However, since $\boldsymbol{Q}^*$ remains unchanged with respect to variations of the sign of $\boldsymbol{w}$, determining $\Omega \in [0, 2\pi]$ requires the knowledge of the direction of motion. For this reason, its values will be restricted to the interval $[0, \pi]$ in this application, but determining the correct interval is immediate once the direction of motion is known.

We use the following error measures:

$$\begin{aligned}
\Delta a &= a - \widehat{a} \\
\Delta e &= e - \widehat{e}, \\
\Delta i &= (180/\pi) \cdot \theta(i, \widehat{i}) \\
\Delta\Omega &= (180/\pi) \cdot \theta(\Omega, \widehat{\Omega}), \\
\Delta\omega &= (180/\pi) \cdot \theta(\omega, \widehat{\omega})),
\end{aligned} \tag{34}$$

where θ measures the signed difference between the two angles.

Scenario 1: a nearly-circular orbit

Since most orbits of interest are nearly circular, we chose a nearly-circular orbit as a first test case for the performance of this purely geometric method. Specifically, we choose the orbit traveled by the satellite of the AQUA mission [22]. Its orbital elements can be found in Table 2.

Table 2. Orbital elements of the AQUA satellite.

a	e	i	Ω	ω
7080.6 km	0.0015	98.20°	95.21°	120.48°

We obtained simulated observer data considering observations gathered by three ground stations rotating with the Earth at different times. Five of the selected observations are represented in Fig. 3.

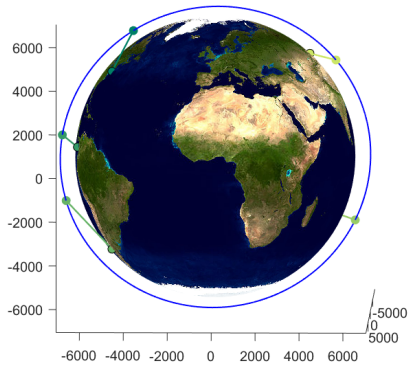

Figure 3. Five observations gathered by three ground stations for the AQUA orbit.

The 10 observers are given in geocentric coordinates, in units of Earth radii, by

$$\big[\boldsymbol{x}_1\big|\cdots\big|\boldsymbol{x}_{10}\big] \approx \begin{bmatrix} .238 & .327 & .399 & .179 & .238 & -.485 & -.006 & -.089 & -.128 & -.186 \\ -.733 & -.913 & -.789 & -.980 & -.733 & .764 & .997 & .989 & .672 & .247 \\ .637 & .243 & .467 & .087 & -.637 & -.426 & .078 & .122 & .729 & .951 \end{bmatrix}.$$

A corresponding set of unit-length bearings is obtained from known points along the AQUA orbit:

$$\big[\boldsymbol{u}_1\big|\cdots\big|\boldsymbol{u}_{10}\big] \approx \begin{pmatrix} -.226 & -.587 & -.443 & -.381 & -.343 & .281 & -.288 & -.014 & .619 & .722 \\ -.755 & -.495 & -.451 & -.486 & -.645 & -.958 & .053 & .907 & .776 & -.624 \\ -.616 & -.641 & -.775 & -.786 & .683 & .060 & -.956 & -.421 & -.122 & .298 \end{pmatrix}.$$

The ground-truth disk quadric $\boldsymbol{Q}^*$ for AQUA is

$$\boldsymbol{Q}^* \approx \begin{bmatrix} .0284 & -.0885 & .1406 & .0002 \\ -.0885 & .9919 & .0128 & -.0007 \\ .1406 & .0128 & .9797 & .0012 \\ .0002 & -.0007 & .0012 & -.8114 \end{bmatrix}. \tag{35}$$

Since the eccentricity of AQUA is $e = 1.5 \times 10^{-3}$, we might expect that the circular model gives a reasonable approximation to the ground-truth. Thus, to obtain a preliminary assessment of the feasibility of using parameter homotopies for this IOD scenario, we considered both the circular and elliptical models. In this experiment, 100 random observer-bearing correspondences were sampled, from a total $120 = \binom{10}{3}$ possibilities for the circular model and $252 = \binom{10}{5}$ for the elliptical model, and the corresponding polynomial systems appearing in Proposition 1 were solved. Average runtimes and errors for this experiment are reported in Table 3. For the circular model, we do not report the argument of periapsis ω since it is undefined.

Table 3 shows that the homotopy solvers for both models run on the order of less than a second. The difference in runtimes by a factor of roughly 5 is due largely to the fact that there are $66/12 = 5.5$ times as

Table 3. Average solver runtime and errors on noiseless AQUA data.

model	avg. runtime	avg. ΔQ^*	avg. Δa	avg. Δe	avg. Δi	avg. $\Delta\Omega$	avg. $\Delta\omega$
circular	$0.13\,\mathrm{s}$	2.2×10^{-3}	$2.4\,\mathrm{km}$	1.5×10^{-3}	$2.8 \times 10^{-2\circ}$	$-1.3 \times 10^{-1\circ}$	-
elliptical	$0.67\,\mathrm{s}$	2.1×10^{-12}	$-2 \times 10^{-3}\,\mathrm{km}$	1.2×10^{-9}	$3.8 \times 10^{-6\circ}$	$-1.6 \times 10^{-6\circ}$	$-8.8 \times 10^{-5\circ}$

many paths to track in the elliptical model vs the circular model. Additionally, we used a very conservative value of 1×10^{-16} for the minimum value of the predictor/corrector stepsize Δt, so as to guard against potential failures when tracking solution paths. This is a particular concern for the ground-truth solution, since the orbit is nearly-circular.

Under the elliptical model, Table 3 shows that we can recover the ground-truth AQUA orbit, from noiseless observations, with high accuracy on average. Errors under the circular model are uniformly higher, but still reasonably small. Figure 4 compares the error distributions for ΔQ^*, Δa, Δi, and $\Delta\Omega$ between both models. Note that Δe is constant for the circular model. When interpreting these results in the noiseless case, it is important to note that the elliptical model, despite providing much smaller errors, will have nearly-singular solutions for nearly-circular orbits like AQUA. As a result, the circular model may sometimes be preferable in such situations.

To illustrate our proposed method of orbit determination on an example from the nearly-circular case, we now focus on a particular set of observers and bearings which appear in Fig. 3, corresponding to columns $1, 4, 5, 6, 9$ in the observer and bearing matrices above. Under the elliptical model, 44 of the 66 complex solutions in recovered by the solver give a real-valued disk quadric. However, only 3 of these real disk quadrics can be lifted to real-valued orbital parameters $(\boldsymbol{w}, \boldsymbol{g}, b)$ (see Rem. 1.) These real solutions are given, modulo the four-fold sign ambiguity, by

$$\begin{aligned}
\boldsymbol{X}_1 &\approx \begin{bmatrix} -1.00 & -.033 & -.022 & .001 & .310 & -.527 & -1.136 \end{bmatrix}, \\
\boldsymbol{X}_2 &\approx \begin{bmatrix} -.970 & -.111 & .216 & .033 & -.068 & .112 & 1.171 \end{bmatrix}, \\
\boldsymbol{X}_3 &\approx \begin{bmatrix} -.986 & -.090 & .143 & .000 & -.001 & .001 & -1.110 \end{bmatrix}.
\end{aligned} \tag{36}$$

The solution $\boldsymbol{X}_3$ corresponds to the ground-truth. To rule out the additional real solution, a sixth line coming from the observation $(\boldsymbol{x}_2, \boldsymbol{u}_2)$ may be used. Evaluating the left-hand side of equation (23) for this line at both solutions $\boldsymbol{X}_1$ and $\boldsymbol{X}_2$ gives residual errors of 3.9×10^{-3}, 4.6×10^{-4}, and 6.2×10^{-16}, respectively. Thus, the solution $\boldsymbol{X}_3$ gives the best fit to the sixth observation.

Applying the circular model to this same example (with observations 1, 5, and 6), there are now 6 real solutions up to sign ambiguity in the nonzero parameters $(\boldsymbol{w}, b)$. However, all 5 original observations may now be used to remove the 7 extraneous solutions. Evaluating the residuals of constraints (23) on these additional solutions as with the elliptical model allows us to distinguish the correct solution. Another comparison between the ground-truth and the extraneous solutions may be obtained by computing the distance from each of the five estimated orbit points to the orbital plane. For the three observations used in the homotopy solver these distances all equal b, but these distances may be significantly different for the two unused observations. For each of the 6 real solutions, we may compute the variance of the set of three distances comprised of b and the unused observations. One of these values is 1×10^{-9}, and the rest are on the order of 1×10^{-3} or higher. This strongly signals the best approximation of the ground-truth solution, which is given by

$$\boldsymbol{X} \approx \begin{bmatrix} -.986 & -.090 & .142 & 0 & 0 & 0 & -1.109 \end{bmatrix}.$$

Scenario 2: an elliptical orbit

As a second test case, we consider an orbit traveled by one of the Magnetospheric Multiscale Spacecrafts (MMS) [23]. This is a highly-elliptical orbit, whose orbital elements we report in Table 4.

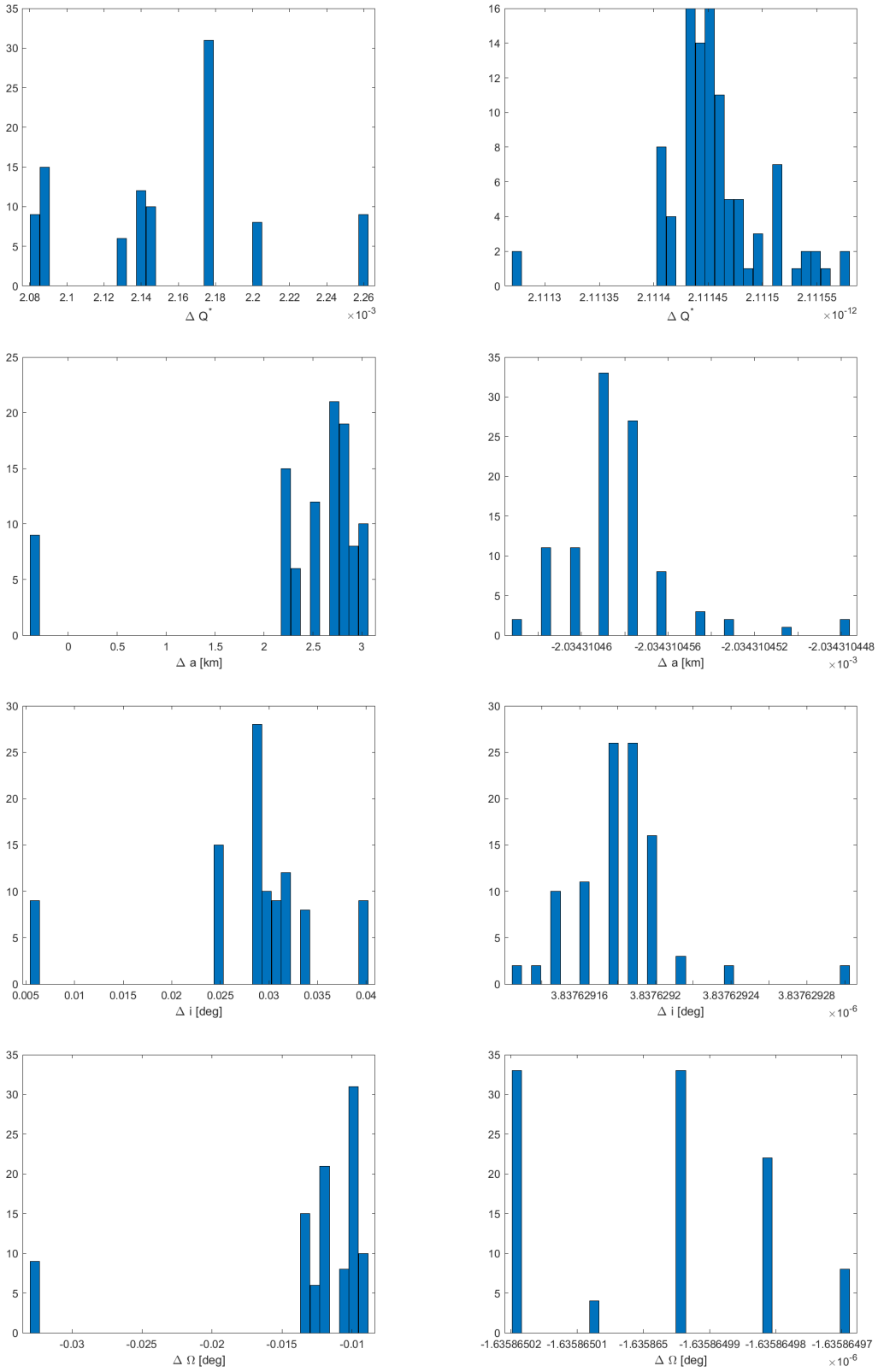

Figure 4. Distribution of $\Delta Q^*, \Delta a, \Delta i, \Delta\Omega$ for noiseless observations from AQUA, with the circular model shown on the left and the elliptical model shown on the right. Note the significantly smaller scales for the elliptical model.

Table 4. Orbital elements of one of the MMS satellites.

a	e	i	Ω	ω
83519.02 km	0.9082	28.50°	357.84°	298.22°

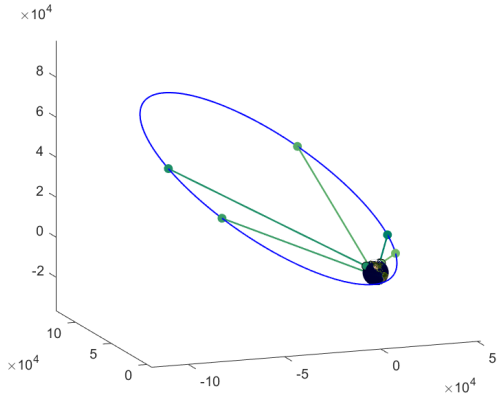

Figure 5. Five observations of the MMS satellite made by three ground stations.

Like the previous scenario, 10 observations were obtained with three ground stations on the Earth's surface, and we evaluated the runtime and accuracy on 100 noiseless observations. The summary statistics shown in Table 5 and Fig. 6 demonstrate that the solver for the elliptical model is efficient and highly accurate in all cases. Note that we do not consider the elliptical model.

Table 5. Average solver runtime and errors on noiseless MMS data.

model	avg. runtime	avg. $\Delta Q*$	avg. Δa	avg. Δe	avg. Δi	avg. $\Delta\Omega$	avg. $\Delta\omega$
elliptical	0.56 s	3.0×10^{-14}	2×10^{-1} km	2.6×10^{-7}	$5.4 \times 10^{-5\circ}$	$-2.8 \times 10^{-7\circ}$	$-4.1 \times 10^{-4\circ}$

Figure 5 shows 5 of the 10 line-of-sight observations for MMS. We use these observations in our Monte Carlo study of noisy observations. Solving the elliptical model yields 11 real solutions in this case, 10 of which can be easily excluded by examining the residuals of a sixth line. With a view towards the model selection problem when the shape of the orbit is not known *a priori*, we also considered what would happen if we solved the circular model for three of these observations. In this short experiment, 4 of the resulting 12 solutions turned out to be real. However, we obtained a strong signal of model mismatch by computing the variances of the estimates of b, which resulted in a value greater than 1 for each solution.

Noisy observations and comparison with other methods

To test the robustness of the homotopy solvers to noise under various scenarios, we consider the following noise model. For each bearing vector $\boldsymbol{u}$, a noisy perturbation $\tilde{\boldsymbol{u}}$ is given by

$$\tilde{\boldsymbol{u}} = \boldsymbol{u} + \epsilon \tag{37}$$

where $\epsilon \sim N(0, \boldsymbol{R})$. That is, ϵ is zero-mean Gaussian noise with covariance following the so-called QUEST measurement model (QMM) [24, 25]

$$\boldsymbol{R} = E[\epsilon\epsilon^T] = \sigma^2 \left(\boldsymbol{I}_{3\times 3} - \boldsymbol{u}\boldsymbol{u}^T\right), \tag{38}$$

where σ is the standard deviation of the bearing error in radians. Note that $\boldsymbol{R}$ is a 3×3 matrix of rank 2, with a null space in the direction of $\boldsymbol{u}$. This means that ϵ lies in the plane normal to $\boldsymbol{u}$. If ϵ is small, then $\tilde{\boldsymbol{u}}$ remains a unit vector to first order.

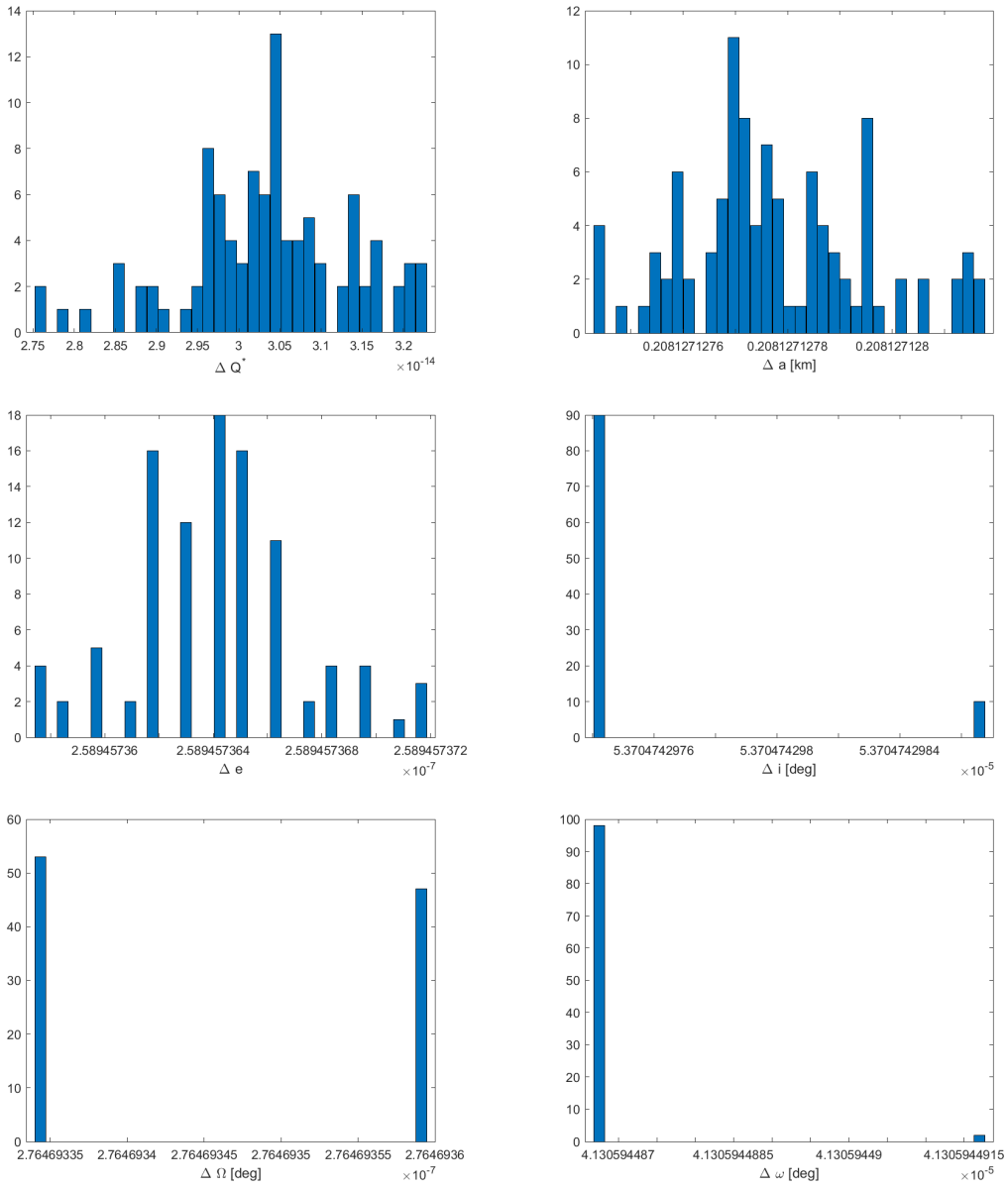

Figure 6. Error distribution of estimated Q^* and orbital elements for noiseless observations from AQUA.

For both the AQUA scenario depicted in Fig. 3 and the MMS scenario in Fig. 5, we ran a Monte Carlo simulation under the noise model described above with 10K runs and $\sigma = 1'$ bearing noise. We compared the results obtained by homotopy continuation with those provided by an implementation of the Double-R method [6]. To initialize the double-R iteration, we used an initial guess of half of the true values of the radius of the position for the MMS satellite and 1/4 of the true slant range for AQUA.

Figure 7 compares the results of our purely geometric approach to Double-R for the MMS orbit. The top-left panel shows that our method estimates the matrix $\boldsymbol{Q}^*$ more accurately. This behavior is reflected in the superior estimation of the semi-major axis, where our maximum error of 2000 km is smaller than the maximum error provided by Double-R, (relative error of 3% against the 6% produced by Double-R.) Our method also provides a better estimates of eccentricity (maximum relative error of 0.53% against 1.18%) and inclination, whose maximum error is comparable with that of Double-R but has significantly less variance. Concerning the estimation of the argument of periapsis, the two methods have comparable performance. The only orbital element which is recovered more accurately by Double-R is the longitude of the node. Still, the maximum relative error for Ω provided by our geometric approach is only 0.3%.

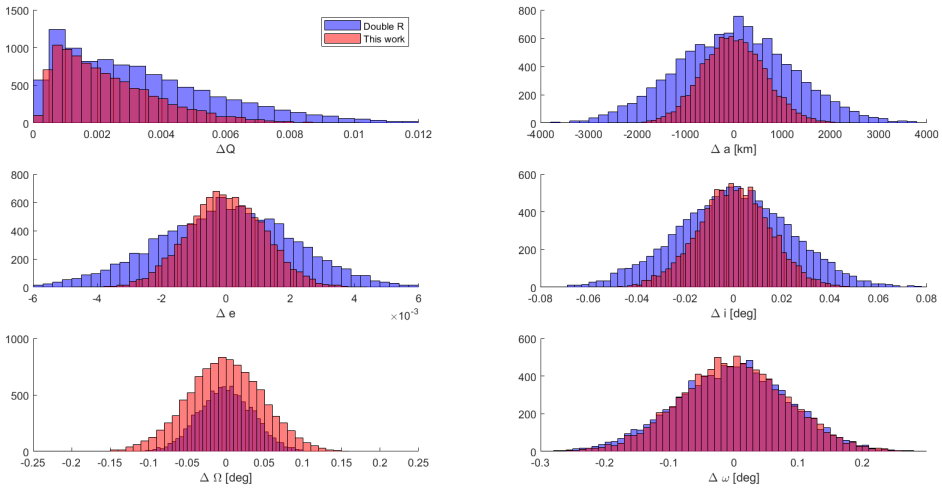

Figure 7. Comparison between the errors produced by the method described in this work and the Double-R iteration method for the MMS orbit under 1 arcmin of noise.

For the AQUA scenario, a comparison of Double-R and our results obtained using the circular model is shown in Fig. 8. The figure shows that Double-R is generally more accurate. Nevertheless, the errors in the solution for our approach are small and concentrated—sufficiently so that this method is likely a good candidate for initializing a Precise Orbit Determination algorithm. We note, however, that the estimates produced by the circular model are biased, most likely due to model mismatch. For comparison, the results produced by applying the elliptical model in presence of noise are represented in Fig. 9. Errors for the elliptical model in this case are appreciably larger than for the circular model. This behavior is expected due to the ground-truth solution being nearly-singular. Unlike the circular model, the results for the elliptical model no longer show any discernible bias.

CONCLUSION

This work develops a purely geometric method for solving the angles-only initial orbit determination (IOD) problem, using only the assumption that the unknown orbit is a conic. Our method is unique in comparison to existing angles-only methods which all, to the best of our knowledge, require propagating the orbit and thus explicitly rely on a dynamical model and on time. Our new method is also immune to various problems

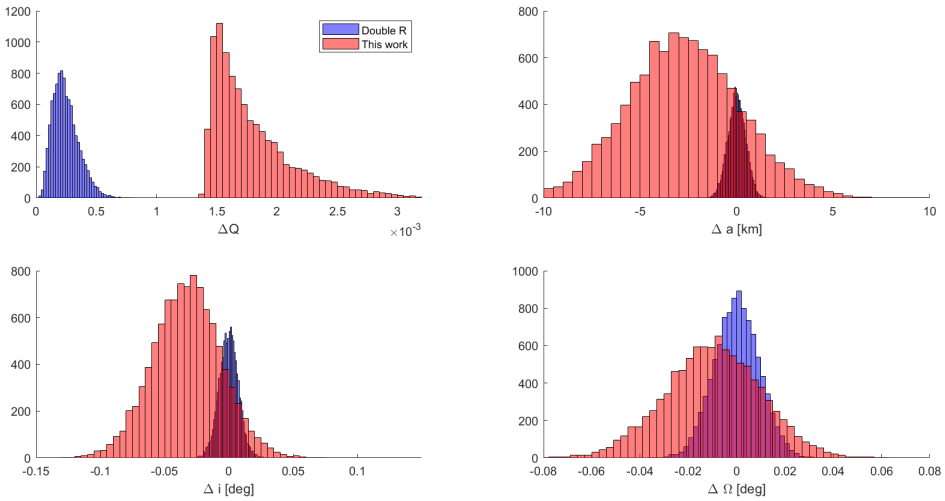

Figure 8. Comparison between the results obtained using the circular model and the Double-R iteration method for the AQUA orbit under 1 arcmin of noise.

affecting the determination of the time-of-flight of an orbiting object between two positions. Standing out among these problems is the light time-of-flight: for our method to work, it is sufficient that the line of observation passes through *any* point on the orbit, and it is not necessary that the body physically passes through the line-of-sight at the time of observation. The extent to which the measured times of flight may differ from the true values depends on the distance of the observed object and is therefore may not always be predictable, especially if no information is available about the orbit.

Experiments demonstrate that our method achieves accuracy that is comparable to, and sometimes better than, one of the standard IOD methods. An attractive feature of using homotopy continuation to solve for the unknown conic $\boldsymbol{Q}^*$ in equations (23) is that it gives a truly global method—no initial guess is required whatsoever. In an additional set of (unreported) experiments, we witnessed for some configurations that the Double-R iteration may have a strong dependence on the initial guesses for the radii. Moreover, poor initialization in general may prevent this method from converging at all. Thus, our approach be used not only as a standalone IOD solver, but also shows potential as a method for providing initial guesses for parameters used by other methods. Such an initialization scheme may increase the accuracy or probability of convergence for these other existing methods.

The experiments also suggest several avenues for further study and improvement of our method. For instance, the source of bias for the circular model, witnessed in Fig. 9, should be more thoroughly investigated. It is also important to address the model selection problem of deciding between circular and elliptical model when the orbit shape is unknown *a priori*. It would be of interest to experiment with other formulations of the problem, which conceivably might allow us to treat the circular and elliptical cases more uniformly. As it stands, a simple approach to model selection would be to try both methods, and then attempt to validate or reject the circular model using the two leftover observations. We have indicated various strategies for implementing such an approach, but more work should be done to test whether they are generally viable. On a similar note, we recall $n = 5$ (or $n = 3$) observations generally only suffice to determine $\boldsymbol{Q}^*$ up to finitely many possibilities, since the systems in Proposition 1 may have several real solutions (with the exact number depending on scenario specifics). We addressed two simple strategies for ruling out "false solutions" using additional observations which would be worthwhile to test further in future work.

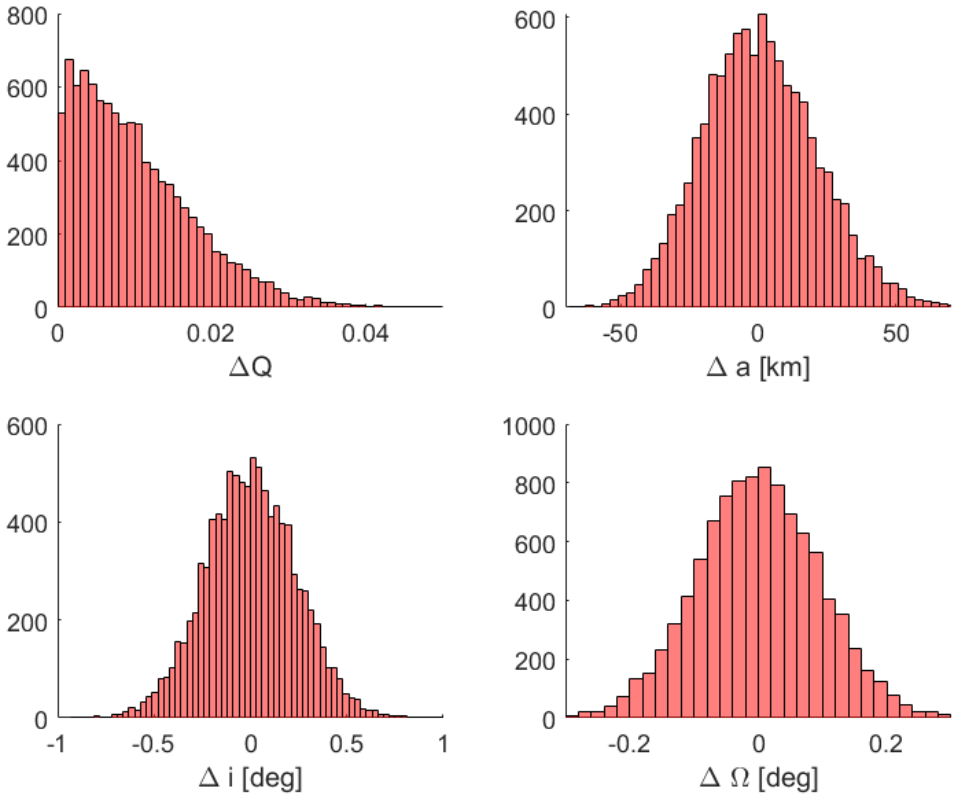

Figure 9. Errors in the estimation of the Q^* matrix and of the orbital elements applying the elliptical model in the AQUA orbit scenario.

ACKNOWLEDGMENTS

The work of T. Duff was supported by the National Science Foundation (NSF) Mathematical Sciences Postdoctoral Research Fellowship (DMS-2103310). The work of M. Mancini and J. Christian was partially supported by the Air Force Office of Scientific Research under the Space University Research Initiative (grant FA95502210092, managed by Dr. Stacie Williams and Dr. Fariba Fahroo). The work of A. Leykin was partially supported by NSF DMS-2001267. The authors greatly appreciate the support of our sponsors.

REFERENCES

[1] C. F. Gauss, *Theoria Motus Corporum Coelestium in Sectionibus Conicis Solem Ambientum*. Hamburg: F. Perthes and I.H. Besser, 1809.

[2] S. Laplace, "Mémoire sur la Détermination des Orbites des Comètes," *Mémoires de Mathématique et de Physique*, 1780, pp. 13–72.

[3] J. Gibbs, "On the Determination of Elliptic Orbits from Three Complete Observations," *Memoirs of the National Academy of Sciences*, Vol. 4, No. 8, 1889, pp. 79–104.

[4] C. L. Hollenberg and J. A. Christian, "Geometric Solutions for Problems in Velocity-Based Orbit Determination," *Journal of the Astronautical Sciences*, Vol. 67, 2019, pp. 188–224, 10.1007/s40295-019-00170-7.

[5] R. H. Gooding, "A new procedure for the solution of the classical problem of minimal orbit determination from three lines of sight," *Celestial Mechanics and Dynamical Astronomy*, Vol. 66, 1997, pp. 387–423.

[6] P. R. Escobal, *Methods of Orbit Determination*. Malabar, FL: Robert E. Krieger Publishing Company, 2nd ed., 1976.

[7] J. G. Semple and G. T. Kneebone, *Algebraic Projective Geometry*. Oxford, UK: Oxford University Press, 1952.

[8] R. Hartley and A. Zisserman, *Multiple View Geometry, 2nd Ed.* Cambridge, UK: Cambridge University Press, 2003.

[9] J. A. Christian, "A Tutorial on Horizon-Based Optical Navigation and Attitude Determination with Space Imaging Systems," *IEEE Access*, 2021, pp. 19819–19853, 10.1109/ACCESS.2021.3051914.

[10] J. A. Christian, H. Derksen, and R. Watkins, "Lunar Crater Identification in Digital Images," *The Journal of the Astronautical Sciences*, Vol. 68, 2021, pp. 1056–1144, 10.1007/s40295-021-00287-8.

[11] J. A. Christian, "Analytic Initial Orbit Determination using Satellite Streaks in Digital Image," *AAS/AIAA Astrodynamics Specialist Conference*, No. AAS 21-789, 2021.

[12] I. R. Shafarevich, *Basic algebraic geometry. 1*. Springer-Verlag, Berlin, second ed., 1994. Varieties in projective space, Translated from the 1988 Russian edition and with notes by Miles Reid.

[13] B. Sturmfels, *Solving systems of polynomial equations*, Vol. 97 of *CBMS Regional Conference Series in Mathematics*. Published for the Conference Board of the Mathematical Sciences, Washington, DC; by the American Mathematical Society, Providence, RI, 2002, 10.1090/cbms/097.

[14] D. A. Cox, J. Little, and D. O'Shea, *Ideals, Varieties, and Algorithms: An Introduction to Computational Algebraic Geometry and Commutative Algebra*. Undergraduate Texts in Mathematics, Springer, Cham, 4 ed., 2015, 10.1007/978-3-319-16721-3.

[15] A. J. Sommese, C. W. Wampler, *et al.*, *The Numerical solution of systems of polynomials arising in engineering and science*. World Scientific, 2005.

[16] A. Leykin, "Numerical algebraic geometry," *J. Softw. Algebra Geom.*, Vol. 3, 2011, pp. 5–10, 10.2140/jsag.2011.3.5.

[17] D. R. Grayson and M. E. Stillman, "Macaulay2, a software system for research in algebraic geometry," Available at `http://www.math.uiuc.edu/Macaulay2/`.

[18] A. P. Morgan and A. J. Sommese, "Coefficient-parameter polynomial continuation," *Appl. Math. Comput.*, Vol. 29, No. 2, part II, 1989, pp. 123–160, 10.1016/0096-3003(89)90099-4.

[19] T. Duff, C. Hill, A. Jensen, K. Lee, A. Leykin, and J. Sommars, "Solving polynomial systems via homotopy continuation and monodromy," *IMA J. Numer. Anal.*, Vol. 39, No. 3, 2019, pp. 1421–1446, 10.1093/imanum/dry017.

[20] T. Duff, V. Korotynskiy, T. Pajdla, and M. H. Regan, "Galois/monodromy groups for decomposing minimal problems in 3D reconstruction," 2021, 10.48550/ARXIV.2105.04460.

[21] C. Améndola, J. Lindberg, and J. I. Rodriguez, "Solving Parameterized Polynomial Systems with Decomposable Projections," 2016, 10.48550/ARXIV.1612.08807.

[22] S. A. Fuselier, W. S. Lewis, C. Schiff, R. Ergun, J. L. Burch, S. M. Petrinec, and K. J. Trattner, "Magnetospheric Multiscale Science Mission Profile and Operations," *Space Science Reviews*, 2014, pp. 77–103, 10.1007/s11214-014-0087-x.

[23] C. L. Parkinson, "Aqua: An Earth-observing satellite mission to examine water and other climate variables," *IEEE Transactions on Geoscience and Remote Sensing*, Vol. 41, No. 2, 2003, pp. 173–183.

[24] M. D. Shuster and S. D. Oh, "Three-axis attitude determination from vector observations," *Journal of Guidance and Control*, Vol. 4, No. 1, 1981, pp. 70–77, 10.2514/3.19717.

[25] M. D. Shuster, "Maximum Likelihood Estimation of Spacecraft Attitude," *The Journal of the Astronautical Sciences*, Vol. 37, No. 1, 1989, pp. 79–88.